

The Impact of Cell Density and Mutations in a Model of Multidrug Resistance in Solid Tumors

James Greene · Orit Lavi · Michael M. Gottesman ·
Doron Levy

Received: 31 May 2013 / Accepted: 29 January 2014 / Published online: 20 February 2014
© Society for Mathematical Biology (outside the USA) 2014

Abstract In this paper we develop a mathematical framework for describing multidrug resistance in cancer. To reflect the complexity of the underlying interplay between cancer cells and the therapeutic agent, we assume that the resistance level is a continuous parameter. Our model is written as a system of integro-differential equations that are parameterized by the resistance level. This model incorporates the cell density and mutation dependence. Analysis and simulations of the model demonstrate how the dynamics evolves to a selection of one or more traits corresponding to different levels of resistance. The emerging limit distribution with nonzero variance is the desirable modeling outcome as it represents tumor heterogeneity.

Keywords Multidrug resistance · Chemotherapy · Mutation · Heterogeneity · Integro-differential equations

1 Introduction

Resistance to chemotherapy is a major cause of the failure of cancer treatment. Our current understanding of drug resistance in cancer is that tumor heterogeneity and complex genetic and epigenetic changes contribute to the development of multidrug resistance (MDR). When this occurs, the cell becomes resistant to a variety of structurally and mechanistically unrelated drugs in addition to the drug initially administered (see Fodal et al. 2011; Gillet and Gottesman 2010).

J. Greene · D. Levy (✉)

Department of Mathematics and Center for Scientific Computation and Mathematical Modeling (CSCAMM), University of Maryland, College Park, MD 20742, USA
e-mail: dlevy@math.umd.edu

O. Lavi · M.M. Gottesman

Laboratory of Cell Biology, National Cancer Institute, National Institutes of Health, Bethesda, MD 20892, USA

Mathematical models have been used to study drug resistance in a variety of circumstances. Furthermore, many important questions have been addressed using different computational approaches, such as: How is early detection and therapy connected with the development of drug resistance? What is the probability that at the time of diagnosis, resistant cancer cells are already present? When several drugs are available, how many drugs should be applied? Should these drugs be used in combination, or sequentially? (see the recent review of Lavi et al. (2012)).

Cancer models include features that influence growth, evolution, MDR and/or intra-tumoral heterogeneity and hence include information about cellular rates. In some cases, these rates can be functions of time, space, density, and/or environmental signals. For instance, consider the natural division rate of cancer cells. The simplest models of cancer growth assume exponential growth (see, e.g., Ledzewicz and Schattler 2006; Panetta 1998), with the growth rate proportional to the current density of cells. This is useful for describing cells in a certain growth phase, but most likely does not hold over their entire lifetime, as it yields unbounded growth. Logistic growth accounts for saturation effects by adding a quadratic competitive interaction term to the growth rate (e.g., see Forys and Marciniak-Czochra 2003; Schuster and Schuster 1995; Stein et al. 2007). The Gompertz growth function, introduced in 1964 by Laird to account for the sigmoidal growth dynamics often observed in tumors, is another prominent choice (see Fister and Panetta 2003; Laird 1964). And other variations exist (for example, see Khain and Sander 2006).

From the above, we see discrepancies in the description of the division rate. Essentially, these models take different forms for their growth rate as a function of cellular density. In fact, other rate parameters often also depend on density, and it is an important aspect of modeling drug resistance. Cell density relates to various factors that determine tumor growth, such as cell–cell interactions, cell–matrix interactions, nutrient distribution, survival signals, the penetration of anti-cancer drugs, and the internal tumor pressure. Many experiments using both normal and cancer cells have directly or indirectly measured the relationship between the rates of cell division and death as functions of cell density, both with and without the administration of a chemotherapeutic agent (Brimacombe et al. 2009; Grantab et al. 2006; Hakanson et al. 2012; Khain and Sander 2006; Long et al. 2003; Nagane et al. 1996; Qiao and Farrell 1999; Saeki et al. 1997; Weaver et al. 2002). In some studies, the cell division rate was found to be a decreasing function of cell density (Hakanson et al. 2012; Khain and Sander 2006), while in others, the reverse was observed (Long et al. 2003; Qiao and Farrell 1999; Saeki et al. 1997). On the other hand, several independent studies have clearly shown that the exact cell death rate depends on the experimental design (Hakanson et al. 2012; Weaver et al. 2002; Zahir and Weaver 2004). Therefore, a theoretical study should examine the properties of these dependencies.

Furthermore, one must also understand how drug resistance is being characterized and choose an appropriate mathematical paradigm to frame the model. Indeed, in the mathematical literature, the problem has been studied for over thirty years. One of the early models of resistance considers the mechanism of point mutations, where cells are in one of two compartments: sensitive or resistant (e.g., see Coldman and Goldie 1985, 1986, 1979, 1983a, 1983b, 1998; Goldie et al. 1982). More advanced stochastic

models of point mutations are found in the reports of Komarova et al. (2006, 2005), while Kimmel et al. (1991, 1990) study gene amplification through branching processes. Continuum-based models are also widely utilized. For instance, ordinary differential equations (ODEs) are employed by Birkhead et al. (1987) to study kinetic resistance and by Tomasetti and Levy (2010) to study point mutations. Michelson and Slate use ODEs to model resistance via increased drug efflux through the ABC transport proteins pathway (Michelson and Slate 1992). Partial differential equation models (PDEs) are also used to describe heterogeneous tumors and vascularization (Jackson and Byrne 2000), and integro-differential equations (IDEs) are sometimes used to describe mutations between sensitive and resistant cancer cells (Lorz et al. 2013).

Lorz et al. (2013) proposed a mathematical model that includes the effects of a continuous variable describing the level of resistance a cell has obtained on cell divisions, apoptosis, and mutation rates of both healthy and cancerous populations. They provide a basis for structured population models including a selection process based on an approach previously developed using partial differential equations (Calsina and Cuadrado 2000, 2004; Champagnat et al. 2006; Desvillettes et al. 2008; Diekmann et al. 2005; Lorz et al. 2011; Magal and Webb 2000; Perthame 2007; Perthame and Barles 2008). Both intratumoral heterogeneity and cellular density were incorporated in the Lorz et al. model. Heterogeneity is described via the resistance variable, and density effects were included only on the growth rate of healthy cells, with cancerous cells having no density dependencies.

In this paper, we aim to develop a mathematical framework for describing MDR by incorporating cell density and mutation dependence. We consider all growth parameters (division, death, and mutation rates, etc.) to be functions of the resistance level (“trait”), which we assume to be a continuous variable. Based on a system of IDEs parameterized by the resistance level, we provide a basis for structured population models designed to estimate the intratumoral heterogeneity over time. Indeed, intratumoral heterogeneity is a widely observed phenomena (Kreso et al. 2013; Marusyk and Cancer 2013; Saunders et al. 2012), but many basic models do not account for it (see Sect. 3). Since cellular density has been proven to have a profound impact on cancer cell dynamics, our study extends the approach of Lorz et al. by including these effects on both natural and drug-induced death rates, in addition to the cell division rate of the cancer cells. Moreover, in our model, the spontaneous death rate is considered to vary in different ways than in Lorz et al. (2013). This results in significantly different net growth and heterogeneity (Figs. 9 and 10). Furthermore, in our model, we account for the occurrence of changes that proceed at higher rates than those of genetic mutations, such as epigenetic changes.

The work is organized as follows. We first provide an overview of the mathematical model in Sect. 2. In Sect. 3 we explore in detail how the mathematical model corresponds to biological observations. We proceed by exhibiting the different behaviors that can be produced by various formulations of the model, together with biological implications. In particular, we move from a model with no density dependence or genetic variation to one that includes both and demonstrate how these features affect tumor heterogeneity. Concluding remarks are presented in Sect. 4.

2 A Mathematical Model for Cancer Dynamics

In deriving the mathematical model, we extend the approach of Lorz et al. (2013). In Lorz et al. (2013), both healthy and cancerous cells are modeled using structured population dynamics that incorporate cell divisions with and without mutations. Healthy cells also include a homeostatic density dependence on the cell division rate only, while cancerous cells are assumed to be able to grow without this inhibitive factor. In this work, we consider cancer cells only, coupled with a drug, which is assumed to be a chemotherapeutic agent, and assume, as is done in Lorz et al. (2013), that the resistance level is described by a scalar, x , which can be normalized such that $x \in [0, 1]$.

Let $n(x, t)$ denote the population density of cancer cells with trait x at time t , and let $\rho(t)$ denote the total number of cells,

$$\rho(t) = \int_0^1 n(x, t) dx. \quad (1)$$

The dynamics of the cancer cell population is then described via the selection/mutation integro-differential equation

$$\begin{aligned} \frac{\partial n(x, t)}{\partial t} = & (f(\rho(t))[r(x)(1 - \theta(x)) - h(D(t), x)] - g(\rho(t))d(x))n(x, t) \\ & + f(\rho(t)) \int_0^1 \theta(y)r(y)M(y, x)n(y, t) dy. \end{aligned} \quad (2)$$

The rationale for Eq. (2) is as follows:

1. $r(x)$ and $d(x)$ denote the natural division rate and death rate of cancer cells with trait x , respectively. We assume that no external forces are influencing the inherent growth and death rates, and hence these rates are constant in time.
2. $D(t)$ represents the dosage of the chemotherapeutic drug at time t , with $h(D(t), x)$ representing the net cytotoxic effect on cancer cells with trait x under dosage $D(t)$. It is common to assume that h increases linearly with drug dosage D , but in certain situations, other forms may be valid. For instance, it may be desirable to include saturation effects in h for large drug concentrations D (for instance, $\lim_{D \rightarrow \infty} h(D, x) = h_1(x) < \infty$ for some function of trait values h_1).
3. The terms $f(\rho(t))$ and $g(\rho(t))$ are included to incorporate density dependence into the division and apoptosis rates. It is well known that both the division and apoptosis rates depend on the cell density (see Bozic et al. 2012; Grantab et al. 2006; Hakanson et al. 2012; Lavi et al. 2012). The specific functional form of these terms plays a key role in the overall dynamics as demonstrated in Sect. 3.
4. The birth ($r(x)$) and drug-induced apoptosis ($h(D(t), x)$) rates have the same density dependence factor f since we are assuming the drug is cell-cycle specific, and hence affects primarily only cells that are dividing. Hence, the induced death term should be proportional to the division rate. This assumption is widely known as the Norton–Simon Hypothesis (Norton and Simon 1977a, 1977b, 1986).

5. All parameters and functions are nonnegative: $r, d, h, g \geq 0$, and $f > 0$ (see Eqs. (6) and (7) below). We also assume that $r, d \in C([0, 1])$. As of now, we make no further assumptions on these terms.
6. We assume that when cells undergo division, they may mutate. That is, if the mother cell has the specific trait x , the daughter cell can have the same trait value x , which we call a faithful division, or it may have a different resistance level y , which we refer to as a mutation. Mutation can either be a permanent genetic change or permanent epigenetic change. The key assumption is that traits are passed down from mother to daughter cell and do not revert back to the original value x after some fixed time.
7. $\theta(x)$ denotes the fraction of cells with trait x undergoing mutation, where $0 \leq \theta(x) \leq 1$, and hence $1 - \theta(x)$ denotes the fraction of cell undergoing faithful division.
8. The last term on the RHS of (2) takes into account all mutations during division from different traits y . $M(y, x)$ denotes the probability that given a mutation, a mother cell with trait y will differentiate into a daughter cell with trait x . As a probability density function, $M(y, x)$ satisfies

$$M(y, x) \geq 0 \quad \forall x, y \in [0, 1], \tag{3}$$

$$\int_0^1 M(y, x) \, dx = 1 \quad \forall y \in [0, 1]. \tag{4}$$

Equation (4) means that since a mutation occurs, it must mutate to some $x \in [0, 1]$.

The notations used in (2) are summarized in Table 1. Equation (2) is a selection and mutation model, which will move through the $(x, n(x, t))$ phase space by both Darwinian evolution and mutations. As time progresses, different gene expressions will become advantageous/disadvantageous, and the overall dynamics will be determined both by the rate and mutation parameters, in addition to the initial distribution of cells. It is important to note that Eq. (2) can be obtained as an expected value of a stochastic model of cells that obey the division/mutation dynamics described above, where the expected value is taken over the number of cells of type x . For the remainder of the paper, we make the following assumptions:

Assumption 1 $D(t) \equiv 1$. This is equivalent to assuming that the drug is applied uniformly in time. A time-dependent $D(t)$ allows one to study treatment protocols, but this is beyond the scope of this work. Hence, we can write the drug-induced rate term $h(D(t), x)$ as a function of the trait value x only, which we define as $c(x)$ ($c(x) := h(1, x)$). As with the other rate parameters $r(x)$ and $d(x)$, we assume the trait dependence on the cytotoxic rate term is continuous, i.e., $c(x) \in C([0, 1])$.

Assumption 2 $\theta(x) \equiv \theta$, a constant. In this work we do not study the effect of the variation of the fraction of mutated divisions on trait value.

Table 1 List of variables

Variable	Range	Biological interpretation
x	$[0, 1]$	Resistance level
t	\mathbb{R}_+	Time
$n(x, t)$	\mathbb{R}_+	Concentration of cells with trait x at time t
$\rho(t)$	\mathbb{R}_+	Density of cells at time t
ρ_f	\mathbb{R}_+	Density of cells at steady state
$r(x)$	\mathbb{R}_+	Natural division rate of cell with trait x
$d(x)$	\mathbb{R}_+	Natural apoptosis rate of cell with trait x
$c(x)$	\mathbb{R}_+	Drug-induced apoptosis rate of cell with trait x
$D(t)$	\mathbb{R}_+	Concentration of drug applied at time t
$f(\rho)$	\mathbb{R}_+	Density dependence on division rate
$g(\rho)$	\mathbb{R}_+	Density dependence on natural apoptosis rate
$\theta(x)$	$[0, 1]$	Proportion of divisions of cells with trait x undergoing mutations
$M(y, x)$	$[0, 1]$	Probability a division results in a mutation from state y to state x given a mutation occurs
Δx	$(0, 1)$	Step-size used in numerical simulations

Substituting Assumptions 1 and 2 into (2) yields the simplified equation

$$\begin{aligned} \frac{\partial n(x, t)}{\partial t} &= (f(\rho(t))[r(x)(1 - \theta) - c(x)] - g(\rho(t))d(x))n(x, t) \\ &\quad + \theta f(\rho(t)) \int_0^1 r(y)M(y, x)n(y, t) dy. \end{aligned} \tag{5}$$

If we define the new timescale $\tau = \int_0^t f(\rho(s)) ds$, then $\frac{\partial n}{\partial t} = \frac{\partial n}{\partial \tau} f(\rho(t))$, and we can rescale (5) to become

$$\begin{aligned} \frac{\partial n(x, \tau)}{\partial \tau} &= (r(x)(1 - \theta) - c(x) - G(\rho(\tau))d(x))n(x, \tau) \\ &\quad + \theta \int_0^1 r(y)M(y, x)n(y, \tau) dy, \end{aligned} \tag{6}$$

where

$$G(\rho) = \frac{g(\rho)}{f(\rho)}. \tag{7}$$

Note that $\frac{d\tau}{dt} = f(\rho(t)) > 0$, so that we have not changed the direction of time. Henceforth, we study (6), with the notational convention that we replace τ by t , even though the change of units is understood as above.

Here, we deal with two cases of initial conditions for (6):

- (i) Uniform distributions in trait x at time $t = 0$, i.e., $n(x, 0) = n_0$, a constant.
- (ii) An initial distribution that is concentrated around some trait $x = x_*$, i.e., $n(x, 0) = B(x) \exp(-|x - x_*|/\epsilon)$, where $0 < \epsilon$. The smaller the ϵ value, the more concentrated the initial distribution is about x_* .

Assuming that $n_0, B(x) \geq 0$, the form of (6) implies that all solutions satisfy $n(x, t) \geq 0$ for all $t \geq 0$ and $x \in [0, 1]$ (see the Appendix for an elementary proof.) Hence, for the remainder of the work, we make these assumptions to ensure positive densities for all time.

3 Analysis and Simulations

In this section we present analytical results and simulation results for Eq. (6). In order to study the relative role of different terms in the model, we study different variants of the model. We start with a trait-based growth model.

3.1 Trait-Based Growth

We first consider the simplified version of (6) where we have no density dependence and no mutations, so the growth solely depends on the cell division and death rates and their response to treatment. Hence, $f \equiv g \equiv 1$, or equivalently, $G(\rho) \equiv 1$, and $\theta = 0$. Thus, Eq. (6) can be written as

$$\frac{\partial n(x, t)}{\partial t} = [r(x) - c(x) - d(x)]n(x, t). \tag{8}$$

We note that Eq. (8) is the model-type used in Lorz et al. (2013) to describe the dynamics of cancer cells. In writing such a model, it is assumed that the cells do not interact in any way, and the growth is dictated solely by the trait x . The solution to (8) is given by

$$n(x, t) = n(x, 0) \exp((r(x) - c(x) - d(x))t) \quad \forall x \in [0, 1], t > 0. \tag{9}$$

In this case, it is trivial to see that the dynamics of the cancer cells in (9) depends on the relation between $r(x) - c(x)$ and $d(x)$. Indeed, if $r(x) - c(x) > d(x)$ and $n(x, 0) > 0$, then $n(x, t) \rightarrow \infty$ as $t \rightarrow \infty$. If $r(x) - c(x) < d(x)$, then $n(x, t) \rightarrow 0$ as $t \rightarrow \infty$. If $r(x) - c(x) = d(x)$, then $n(x, t) \equiv n(x, 0)$ for all $t \in \mathbb{R}_+$. Finally, if $n(x, 0) = 0$, then $n(x, t) = 0$ for all $t > 0$. This last case can be ignored by assuming that $n(x, 0) > 0$ for all $x \in [0, 1]$. This is a technical assumption that simplifies the presentation of the following results. Hence, we are left with only two qualitatively distinct scenarios, which are described by the below theorem:

Theorem 1 Consider the system described by (8) with initial condition $n(x, 0)$. If $r(x) - c(x) < d(x)$ for all $x \in [0, 1]$, then

$$\rho(t) \xrightarrow{t \rightarrow \infty} 0, \quad n(x, t) \xrightarrow{t \rightarrow \infty} 0 \quad \forall x \in [0, 1]. \tag{10}$$

An analogous statement holds if $r(x) - c(x) \leq d(x)$ with $r(x) - c(x) = d(x)$ at a countable number of points x_* , where we will have $n(x_*, t) \equiv n(x_*, 0)$. On the other hand, if there exists $x \in [0, 1]$ such that $r(x) - c(x) > d(x)$, then the solutions satisfy

$$\rho(t) \xrightarrow{t \rightarrow \infty} \infty, \quad \frac{n(x, t)}{\rho(t)} \xrightarrow{t \rightarrow \infty} \sum_{i=1}^m a_i \delta(x - x_i), \tag{11}$$

where $\delta(x)$ denotes the Dirac distribution, the $a_i > 0$ are constants such that $\sum_{i=1}^m a_i = 1$, and the x_i satisfy

$$x_i = \arg \max_{0 \leq x \leq 1} (r(x) - c(x) - d(x)). \tag{12}$$

For a proof, see the [Appendix](#). The above theorem and proof are analogous to Lorz et al. (2013, Lemma 2.2). Note that m denotes the number of points where the maximum is achieved. The constants a_i in the limiting distribution of $n(x, t)/\rho(t)$ must add to one, since this is a probability distribution. Generally, since the initial conditions may be nonhomogeneous, the constants a_i are not equal to each other. In this case, the relative growth in each population will depend on the fraction of initial cells with the corresponding trait. That is, $a_i = n(x_i, 0)/\sum_i^m n(x_i, 0)$.

Theorem 1 implies that (8) can only describe two different growth phenomena: extinction or unbounded growth. In the case of modeling the evolution of cells with a resistant gene, both cases have serious limitations. Extinction, while desirable, is unlikely, and unbounded growth is not biologically feasible. It is well known that even cancer cells, which of course experience less inhibition to growth signals due to cellular pressure and a lack of resources, experience homeostatic forces which slow their division rate (e.g., see Hakanson et al. 2012). Accordingly, Eq. (8) is ill-equipped for studying the growth properties of tumor cells. It is however worth noting that there still is some merit in using such a model when comparing the dynamics of cancerous cells to normal tissue, as the cancer cells may follow a pattern of unlimited growth, at least when compared with healthy cells.

Even with the described limitations however, (8) can describe a rudimentary model of selection. Theorem 1 implies that such a model selects the traits with the maximum net growth rate. That is, all of the x that maximize $r(x) - c(x) - d(x)$ are selected. Hence, even though (8) provides an overall unrealistic modeling environment, it does capture some important phenomena.

To understand how the dynamics evolve, we provide numerical simulations. For this and all future simulations, we will use a standard collocation method of Sinc basis functions on the interval $[0, 1]$ with an equally spaced partition of $k = 4000$ points (see Bellomo 1997 for a basic introduction to the method). That is, we approximate $n(x, t)$ by $n_k(x, t)$, which are defined by

$$n_k(x, t) := \sum_{i=1}^k S_i(x)n_i(t), \tag{13}$$

where $n_i(t) := n(t, x_i = i \Delta x)$, x_i is a fixed point in the partition, and $S_i(x)$ is the function

$$S_i(x) := \begin{cases} \frac{\sin((\pi/\Delta x)(x-i \Delta x))}{(\pi/\Delta x)(x-i \Delta x)} & \text{for } x \neq i \Delta x, \\ 1 & \text{for } x = i \Delta x. \end{cases} \tag{14}$$

Here Δx is the step-size of the partition ($\Delta x = 1/3999$ in our simulations). Note that $S_i(x_i) = 1$ and $S_i(x_j) = 0$ for $i \neq j$. Substituting this approximation (13) into (8) (or later on, the more general (6)), yields a system of ODEs for the $n_i(t)$, which we solve

Table 2 Parameter values used in simulations

Figure	Equation	Parameter values
1	(8)	$r(x) = \frac{2}{1.1+2x^5}, c(x) = \frac{2}{1+x^2}, d(x) \equiv 0.05$
3	(16)	$r(x) = \frac{2}{1.1+2x^5}, c(x) = \frac{2}{1+x^2}, d(x) \equiv 0.05, G(\rho) = \rho(1 - \rho)^2$
4	(16)	Same as in Fig. 3
5	N/A	$r(x) - c(x) = -5x^2 + 6x - \frac{6}{5}, d(x) \equiv 2$
6	(16)	$r(x) - c(x) = -5x^2 + 6x - \frac{6}{5}, d(x) \equiv 2, G(\rho) = \rho(1 - \rho)^2$
7	(16)	Same as in Fig. 6
8	N/A	$r(x) - c(x) = -5x^2 + 6x - \frac{6}{5}, d(x) = \begin{cases} x & \text{if } x \leq \frac{14}{5} \\ \frac{0.0352}{x^{14}} & \text{if } x > \frac{14}{5} \end{cases}$
9	(8)	$r(x) - c(x)$ and $d(x)$ as in Fig. 8
10	(16)	$r(x) - c(x)$ and $d(x)$ as previous, $G(\rho) = \rho(1 - \rho)^2$
11	(16)	Same as in Fig. 10
12	(31)	$r(x) = \frac{2}{1.1+2x^5}, c(x) = \frac{2}{1+x^2}, d(x) \equiv 0.05, G(\rho) = \rho(1 - \rho)^2, \epsilon = 0.01, \theta = 0.1, \tilde{M}$ as in Eq. (30)
13	(31)	Same as in Fig. 12
14	(31)	$\epsilon = 0.01, \theta = 0.1, 0.4, 0.7, 1$. All other parameters are identical to Fig. 12
15	(31)	$\epsilon = 0.1, \theta = 0.1, 0.4, 0.7, 1$. All other parameters are identical to Fig. 12

by standard Runge–Kutta methods. For example, in the case of Eq. (8), the system of ODEs is given simply by the original equation

$$\frac{dn_i(t)}{dt} = [r(x) - c(x) - d(x)]n_i(t). \tag{15}$$

In the full IDE case (6), the analogous expression is more complicated, but is still an ODE with coefficients involving $\int_0^1 S_i(x) dx$, which, once computed initially, are constants.

We would also like to briefly discuss the form of the rate parameters. A common characteristic for $r(x)$ and $c(x)$ to both possess is to decrease as the resistance x increases (see Brimacombe et al., Kreso et al. 2009, 2013). As x increases, the cell becomes more resistant, so by definition the drug-induced kill-term $c(x)$ should decrease for resistant cells. It is less obvious how $d(x)$ should vary with x . In some biological situations, such as the accumulation of mutations, $d(x)$ may increase. On the other hand, in the case of epigenetic changes that reduce the division rate, the death rate could be reduced. In fact, it may not be a monotone function at all. Hence, when studying such a problem, it is important to identify which mechanism or mechanisms are under investigation, so as to accurately represent the respective rates.

Currently, we assume a simple constant form for $d(x)$ and consider uniform initial conditions. The results are independent of this choice of initial conditions. As long as $n(x, 0) > 0$ for all $x \in [0, 1]$, the same asymptotic behavior is achieved (In this case, since mutations are not allowed, if $n(x, 0) = 0$ for some $x \in [0, 1]$, then growth will never occur at such x , and thus the asymptotic behavior could be different. Such is the case if $n(x_*, 0) = 0$ for a maximizer x_* of $r(x) - c(x) - d(x)$). The explicit

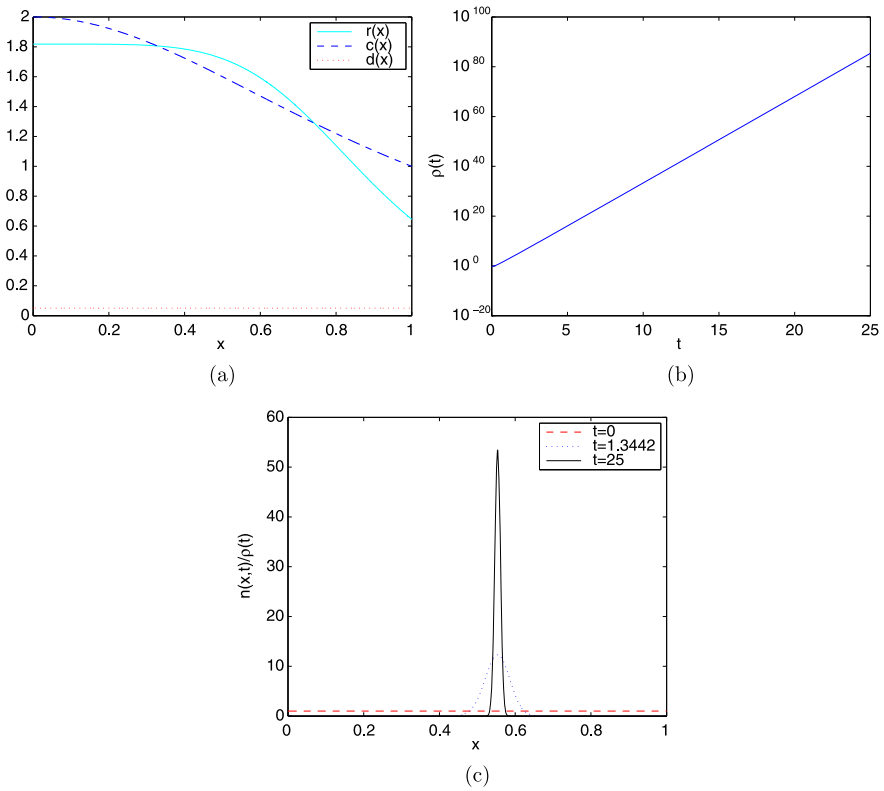
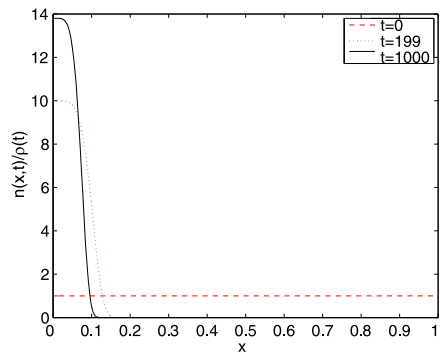


Fig. 1 Numerical results of (8): (a) shows the rate profiles used; (b) a semi-log plot of the evolution of the density ρ ; (c) $n(x, t)/\rho(t)$ as a function of x at three representative times t . Note that in the simulations we have made the time scale change $t \rightarrow t\epsilon^{-1}$, where $\epsilon = 10^{-2}$, since we are primarily interested in studying the long-time behavior of the solution (Color figure online)

functional forms and parameter values used in all simulations are given in Table 2. The simulation results are shown in Fig. 1. Here, the second part of Theorem 1 applies, where there exists x such that $r(x) - c(x) - d(x) > 0$. Theorem 1 then implies that we should have unbounded growth of the total population size $\rho(t)$ and that the growth should concentrate around the x values that maximize $r(x) - c(x) - d(x)$ (Fig. 1(a) shows that this value x_* is in fact unique in this simulation). Figures 1(b) and 1(c) verify the conclusions of the theorem in this case. That is, $\rho(t)$ in Fig. 1(b) demonstrates exponential growth, and $n(x, t)$ in Fig. 1(c) appears to approach a Dirac mass about the value x_* as t grows.

For comparison, we also provide simulations for the case of no treatment, i.e., we study (8) with the same parameter values, except here $c(x) \equiv 0$. As in Fig. 1 (specifically Fig. 1(b)), the density $\rho(t)$ diverges, and in fact diverges much more quickly than the Fig. 1 case. This is of course because the net growth rate is $r(x) - d(x)$, which is larger than the case where the drug was applied, where this rate is $r(x) - c(x) - d(x)$. In more plain terms, the drug inhibits the overall growth of the tumor, which is what we would expect. To keep the numerics within MATLAB

Fig. 2 Numerical results of (8) with $c(x) \equiv 0$, and the same parameters appearing in Fig. 1. Shown is $n(x, t)/\rho(t)$ as a function of x at three representative times t (Color figure online)



tolerances, we simulate $n(x, t)/\rho(t)$. The results are shown in Fig. 2. We see that the model is selecting the $x = 0$ trait asymptotically, which is what we would expect both from Theorem 1 since the maximum of $r(x) - d(x)$ occurs at $x = 0$. Biologically this makes sense, since there is no evolutionary advantage to having a higher x value when the drug is applied. We last note that the time scale in these simulations is much longer than in Fig. 1 because $r(x) - d(x)$ is relatively flat near $x = 0$, and thus it takes longer to visually see the selection occur.

Clearly these figures do not represent a general case, as multiple maximizers of $r(x) - c(x) - d(x)$ could exist. Even if we assume that $r(x)$ and $d(x)$ are both decreasing, there could still be multiple or no points of intersection between them. Given that in general there are no standard assumptions on $d(x)$, the limiting distribution could be any number of Dirac masses, or cell extinction.

3.2 Density-Dependent Model

We next consider a generalization of (8) to which we include competition and/or cooperation among the cells via density effects, but still do not allow for mutations to occur during division. We recall that Lorz et al. (2013) used a specific form of this model (both with and without mutations) to describe healthy cells, while here we use this more general form to describe cancerous cells. In reference to our original model (6), we set $\theta = 0$ and let $G(\rho) \neq 1$ generally. Thus, Eq. (6) takes the form

$$\frac{\partial n(x, t)}{\partial t} = [r(x) - c(x) - G(\rho)d(x)]n(x, t). \tag{16}$$

Similarly to (8), (16) is an ODE for any x . However, due to the density dependence through the term $G(\rho)$, the ODEs in (16) are nonlinear and coupled. Due to these two characteristics, Eq. (16) has more complex dynamics than the trait-based growth only model (8).

We recall that $G(\rho) = g(\rho)/f(\rho)$, where f is the birth-rate density dependence, and g is the natural death-rate density dependence. We assume that in the limit of high density, the growth rate of the cells rapidly decays. More precisely,

$$\lim_{\rho \rightarrow \infty} \frac{f(\rho)}{g(\rho)} = 0^+ \quad \text{or, equivalently,} \quad \lim_{\rho \rightarrow \infty} G(\rho) = \infty. \tag{17}$$

The form of Eq. (17) guarantees that if the natural death-rate g decays to zero in the limit of large cell density, then the birth-rate f will decay even more rapidly. This condition hence prohibits unbounded growth as stated in the following Theorem 2, which is proven in the [Appendix](#):

Theorem 2 *Consider the system described by (16). If $G(\rho)$ satisfies (17), then there exists $\rho_M > 0$ such that*

$$0 \leq \rho(t) \leq \rho_M \quad \forall t \geq 0. \quad (18)$$

The conclusion of Theorem 2 is in fact one of the main motivating factors in introducing density effects into our models. It allows for bounded, nonzero populations to exist, which is biologically (and mathematically) desirable when modeling solid tumor growth. This should be compared with Theorem 1, where the only two outcomes were extinction and unbounded growth.

To demonstrate the difference between Eqs. (8) and (16), we simulate (16) with the same trait dependencies as in Fig. 1(a). We use the following generic choice for $G(\rho)$:

$$G(\rho) = \rho(\rho - 2)^2. \quad (19)$$

Note that (19) satisfies (17), so that Theorem 2 applies. The simulation results of (16) are shown in Figs. 3 and 4. For a direct comparison with Fig. 1, uniform initial conditions are used, although the long-time dynamics would still remain unchanged with any initial conditions satisfying $n(x, 0) > 0$ for all $x \in [0, 1]$.

Figures 3(a) and 1(c) exhibit the same selection, that is, growth that limits to a monoclonal population with trait x_* . However, comparing Figs. 1(b) and 3(c), we see an important difference. Namely, instead of having unbounded growth in the total population as given by Eq. (8), we now have, via Theorem 2, bounded populations. In fact, in Fig. 3(c), we see that $\rho(t)$ converges to an asymptotic profile. In contrast to Lorz et al. (2013), cancer cells are described with bounded growth, while previously, they could only diverge or become extinct. For the brevity and clarity of the presentation, we only show simulation results for $t = 2$. Analogous results are obtained for longer times.

To understand the dynamics portrayed by Fig. 4(a) (and Fig. 3(b) for snapshots in time), we consider a population with density $\rho(0) = 1$. In this case, the growth rate is $r(x) - c(x) - G(1)d(x)$. Due to the initial conditions and the growth parameters $r(x)$, $c(x)$, and $d(x)$, initially we observe a decrease in $\rho(t)$. $G(\rho)$ given by (19) increases, pushing $G(\rho)d(x)$ upwards. However, the effect of the populations growing exponentially where $r(x) - c(x) - G(\rho)d(x) > 0$ outweighs the increase of populations with a negative division rate, and we quickly see an increase in $\rho(t)$. The product $G(\rho)d(x)$ decreases until $\rho = 2$, where the growth is most rapid, followed by a slowing down of $\rho(t)$ as $G(\rho)d(x)$ increases as it reaches the peak of $(r - c)(x)$. Note that the limiting behavior adapts to the growth rate, density, and population values satisfying the following relations:

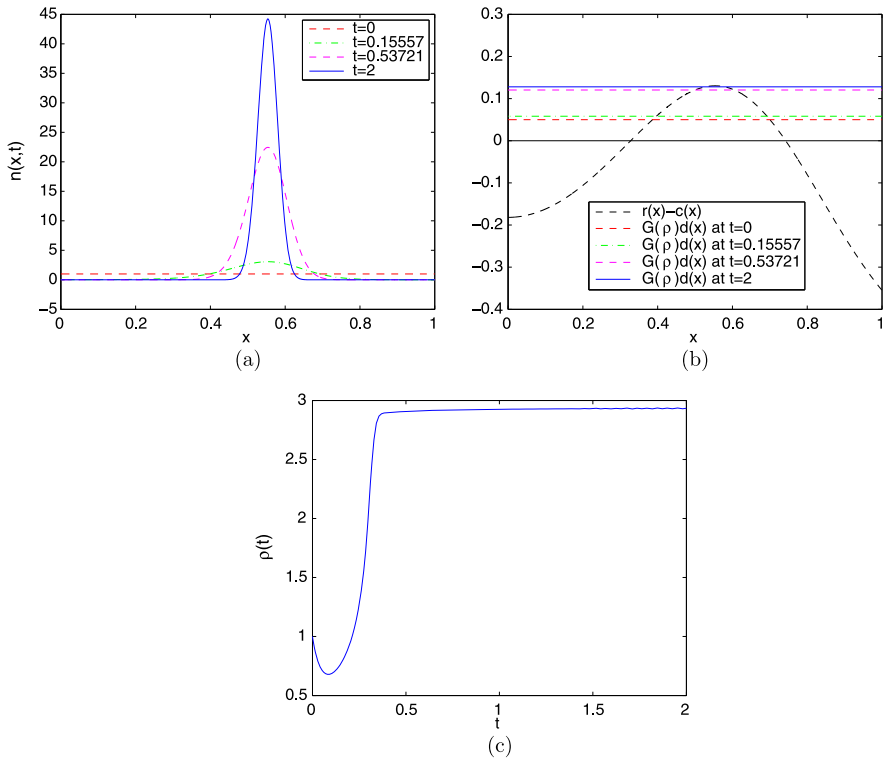


Fig. 3 Simulations of (16) using trait parameters and time scale as in Fig. 1. G is given by (19). (a) The profiles of $n(x, t)$ at four times t ; (b) the variation of the net-growth rates as the density changes in time, at the same four times used in (a); (c) evolution of the density $\rho(t)$ (Color figure online)

$$\lim_{t \rightarrow \infty} \rho(t) = \rho_*, \tag{20}$$

$$G'(\rho_*) > 0, \tag{21}$$

$$r(x) - c(x) - G(\rho_*)d(x) < 0 \quad \forall x \neq x_*, \tag{22}$$

$$r(x_*) - c(x_*) - G(\rho_*)d(x_*) = 0, \tag{23}$$

and

$$n(x, t) \xrightarrow{t \rightarrow \infty} \rho_* \delta(x - x_*). \tag{24}$$

Properties (22) and (23) are most readily seen in Fig. 3(b) where the line $G(\rho)d(x)$ is essentially tangent to the $r(x) - c(x)$ curve at its maximum value x_* at $t = 2$. Properties (20)–(24) provide a way to understand the general dynamics of (16). An analogous statement holds if there exists multiple x_* satisfying (23).

The evolution of the population in this example is then similar to the population described by (8), except that the net growth rate adapts to bound the total population, leading to the convergence of $\rho(t)$. Indeed, this is an important biological characteristic that makes (16) a more suitable model.

Adding a density dependence can result in even richer dynamics. For example, consider the dynamics of both (8) and (16) with rate parameters shown in Fig. 5,

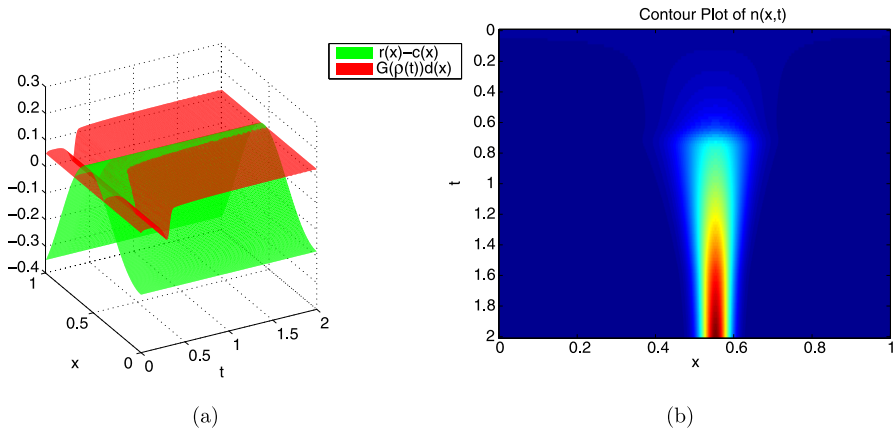
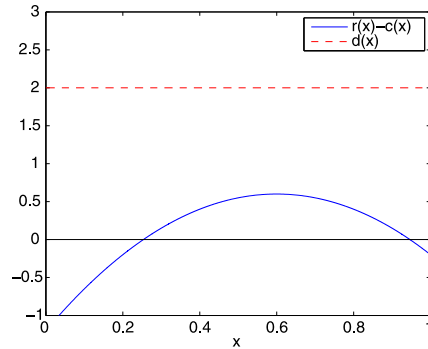


Fig. 4 Simulations of (16) using trait parameters and time scale as in Fig. 1 and G is given by (19). (a) The net-growth rates as a surface plot over t and x ; (b) is a contour plot of $n(x, t)$ (Color figure online)

Fig. 5 $r(x) - c(x)$ and $d(x)$ used for Figs. 6 and 7. Only the difference between $r(x)$ and $c(x)$ is plotted since that is the term that controls the dynamics in all models. Note that $r(x) - c(x) < d(x) \forall x \in [0, 1]$ (Color figure online)



where $G(\rho)$ is given by (19). The dynamics of (8) are clear: since $r(x) - c(x) - d(x) < 0$ for all $x \in [0, 1]$, all the populations go extinct exponentially. That is: $\rho(t) \rightarrow 0$ and $n(x, t) \rightarrow 0$ for all $x \in [0, 1]$ as $t \rightarrow \infty$.

However, the dynamics of (16) are qualitatively different, as shown in Figs. 6 and 7. Here we see, as in the case of Eq. (8), an initial decay of $n(x, t)$ for all x and hence a decrease in $\rho(t)$. However, the function $G(\rho)d(x)$ initially increases, causing an even faster decay of $\rho(t)$. As $\rho(t)$ approaches 0, $G(\rho)$ given by (19) also decreases. Eventually, by the continuity of G and the fact that $G(0) = 0$ and that there exists x such that $r(x) - c(x) > 0$, ρ diminishes enough so that we have x such that $r(x) - c(x) - G(\rho)d(x) > 0$. Consequently, such cell populations begin to grow, leading to an increase in $\rho(t)$. The entire population is thus prevented from dying out, and the limiting dynamics are again described by (20)–(24), where the new ρ_* and x_* are determined by the trait and density parameters and by the initial conditions.

It is important to note that the reason the population does not die out in Figs. 6 and 7 is because $G(0) = 0$. If the population approaches $\rho = 0$, the fact that there exists x where $r(x) - c(x) > 0$ allows us to conclude that there will be some cells that will

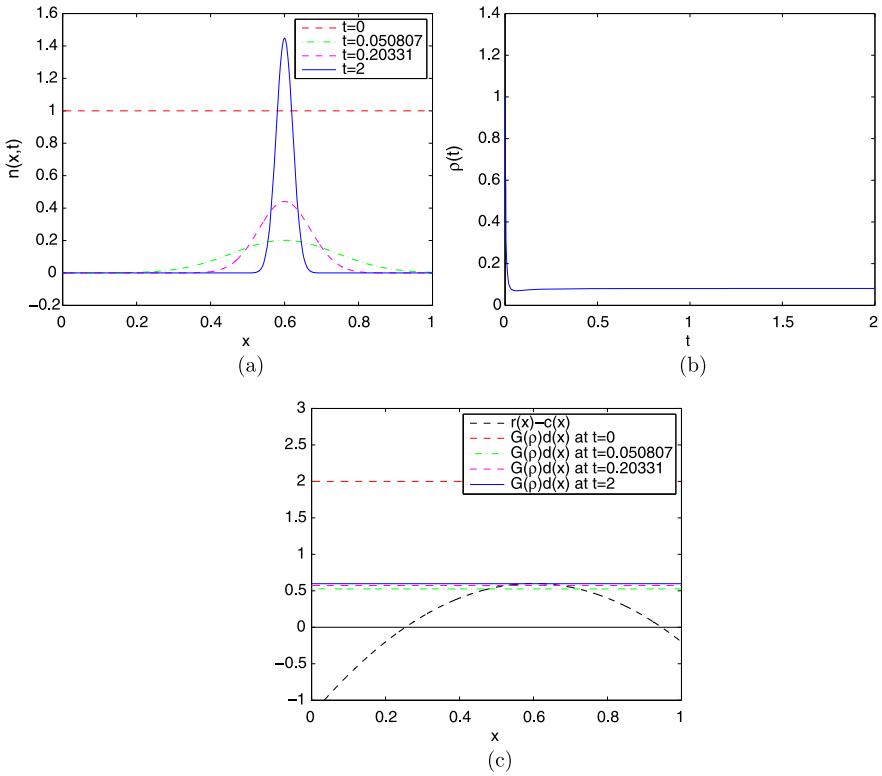


Fig. 6 Simulations of (16) using the trait parameters shown in Fig. 5. G is given by (19). The time scale as in Fig. 1. **(a)** The profiles of $n(x, t)$ at four representative times; **(b)** the evolution of the density; **(c)** the variation of the net-growth rates as the density changes in time, at the same four times used in **(a)** (Color figure online)

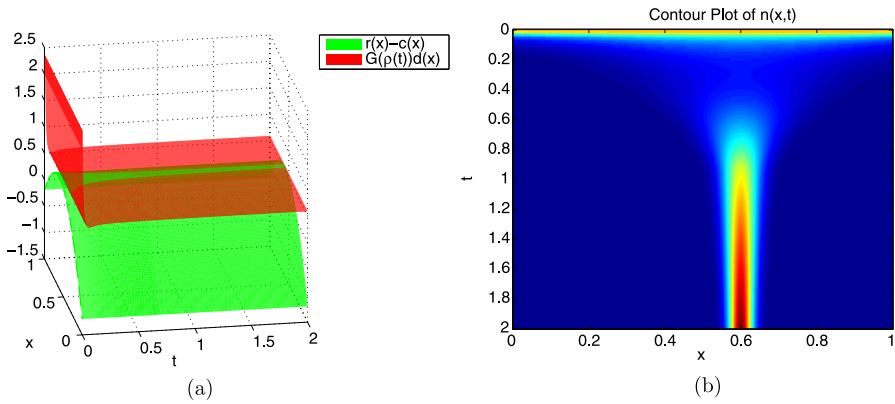


Fig. 7 Simulations of (16) with the trait parameters shown in Fig. 5. G is given by (19). The time scale are identical to those in Fig. 1. **(a)** A surface plot of the net-growth rates; **(b)** a contour plot of $n(x, t)$ (Color figure online)

Fig. 8 $r(x) - c(x)$ and $d(x)$ used for Figs. 9–11. Note that $\arg \max_{0 \leq x \leq 1} (r(x) - c(x) - d(x)) = 0.5$ and that $r(0.5) - c(0.5) - d(0.5) > 0$ (Color figure online)

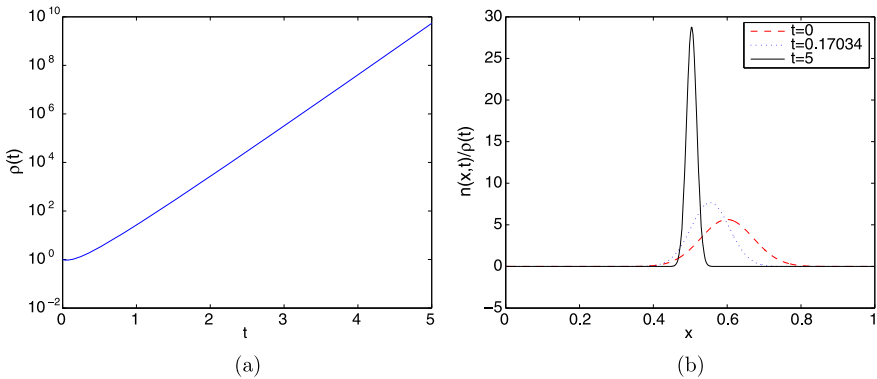
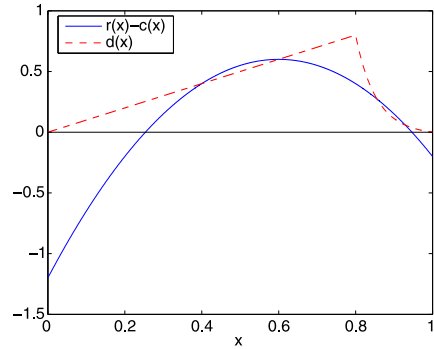


Fig. 9 Simulations of (8) using rates shown in Fig. 8. (a) A semi-log plot of the evolution of the density ρ ; (b) the profiles of $n(x, t)$ at three representative times. Note that in the simulations we have made the time scale change $t \rightarrow t\epsilon^{-1}$, where $\epsilon = 10^{-2}$, since we primarily are interested in the long-time behavior (Color figure online)

begin to grow. If, for biological reasons, $G(0) > 0$, then it is entirely possible to have $\rho(t) \rightarrow 0$.

Incorporating a density dependence into the mode may also result in a selection of different trait values x . Consider the same density dependence $G(\rho)$ as in (19), with $r(x)$, $c(x)$, and $d(x)$ that are shown in Fig. 8 (and Table 2). For Eq. (8), Theorem 1 implies that we have selection toward value(s) x_* that maximize $r(x) - c(x) - d(x)$, which by our choice is unique and given as $x_* = 0.5$, i.e., $\rho(t) \rightarrow \infty$ and

$$\frac{n(x, t)}{\rho(t)} \xrightarrow{t \rightarrow \infty} \delta(x - x_*) \tag{25}$$

This is demonstrated in Fig. 9. Note that pointwise we still have growth in other populations with $x \neq x_*$, but not nearly as fast. For instance, the populations with $x \approx 0.9$ grow exponentially, but not as rapidly as those with $x = x_*$. Even with concentrated initial distributions that were assumed here, as opposed to uniform, the same long-time dynamics emerge in both cases.

The solution of (16), shown in Figs. 10 and 11, has a different selection strategy. We see that, as in (8), initially the trait with the highest growth rate is $x_* = 0.5$, and

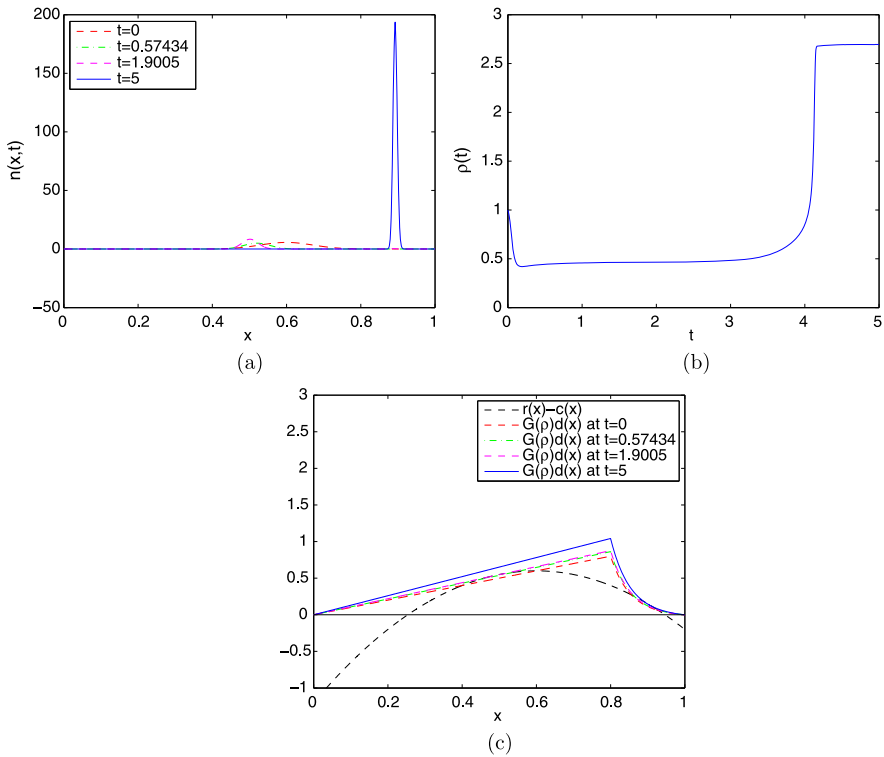


Fig. 10 Simulations of (16) using the trait parameters shown in Fig. 8. G is given by (19). (a) The profiles of $n(x, t)$ at four representative times; (b) the evolution of the density; (c) the variation of the net-growth rates as the density changes in time, at the same four times used in (a). Note that in the simulations we have made the time scale change $t \rightarrow t\epsilon^{-1}$, where $\epsilon = 10^{-2}$, since we primarily are interested in the long-time behavior (Color figure online)

the population appears to grow monoclonally. However, as can be seen in Fig. 11(a), there is still a region near $x \approx 0.9$ where $r(x) - c(x) > G(\rho)d(x)$, and thus there, exponential growth is still occurring. Recalling (20)–(24), the curve $G(\rho)d(x)$ must continue to increase in order for (22) to hold for all but a finite number of x . Hence, ρ continues to increase, eventually growing so large that $r(0.5) - c(0.5) < G(\rho)d(0.5)$, causing the death of the $x = 0.5$ cells. In the limit, (22) holds for all x except $x_* = 0.8925$, and we have

$$\lim_{t \rightarrow \infty} n(x, t) = \rho_* \delta(x - x_*),$$

as can be seen in Fig. 10(a) or Fig. 11(a). We see from Fig. 10(b) that $\rho_* \approx 2.6$, which means that the inclusion of the density dependence results with the selection of a different trait. Hence, the choice of the model paradigm for cancer cells is important, with qualitatively different dynamics in the distinct frameworks.

3.3 Selection/Mutation Model

As discussed in Sect. 3.2, by adding a density dependent cooperation/competition term, we were able to model systems of cells with nonzero yet finite limiting total

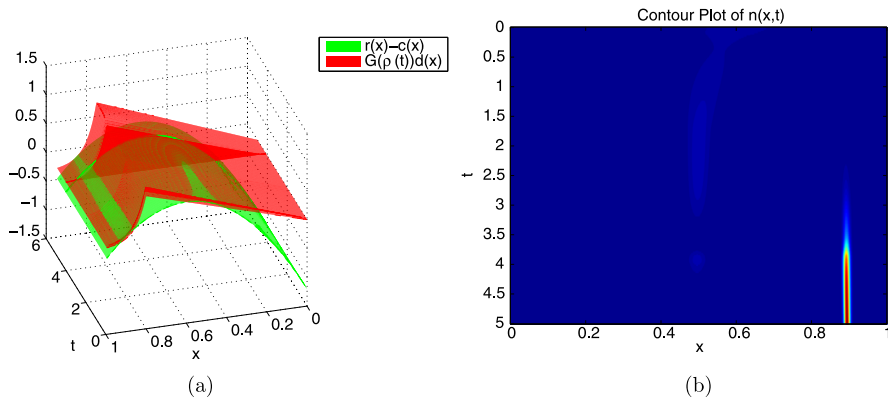


Fig. 11 Simulations of (16) with trait parameters in Fig. 8. G is given by (19). (a) The net-growth rates as a surface plot over t and x ; (b) a contour plot of $n(x, t)$. Note that in the simulations we have made the time scale change $t \rightarrow t\epsilon^{-1}$, where $\epsilon = 10^{-2}$, since we primarily are interested in the long-time behavior (Color figure online)

populations, something that is not possible in the simple model (8). Adding a density dependence was shown to result in richer underlying dynamics. Yet, the asymptotic behavior of (16) always satisfies the following: given that $\exists \rho_* > 0$ such that $\rho(t) \rightarrow \rho_*$, $\exists m \in \mathbb{N}$, $m < \infty$, $\{x_i\}_{i=1}^m \in [0, 1]$, and $\{a_i\}_{i=1}^m \in \mathbb{R}_+$ such that

$$\lim_{t \rightarrow \infty} n(x, t) = \sum_{i=1}^m a_i \delta(x - x_i),$$

where $\sum_{i=1}^m a_i = \rho_*$. Equivalently,

$$\lim_{t \rightarrow \infty} \frac{n(x, t)}{\rho(t)} = \sum_{i=1}^m a'_i \delta(x - x_i), \tag{26}$$

where $0 < a'_i \leq 1$ and $\sum_{i=1}^m a'_i = 1$. In other words, there exists only a finite number of traits that exist asymptotically, with all other populations dying out. Such a result, while an improvement over the dynamics of (8), is in contradiction to intratumoral heterogeneity observations. We expect to see a stable distribution centered around a finite number of traits, with wider variance around such traits. It is worth noting also that the a_i (or a'_i) have a more complex relationship to the initial population values $n(x, 0)$, as opposed to when they were seen in (8). This added complexity is due to the density dependence.

With this in mind, we introduce our full model given by Eq. (6), which we repeat here for convenience:

$$\begin{aligned} \frac{\partial n(x, t)}{\partial t} &= (r(x)(1 - \theta) - c(x) - G(\rho(t))d(x))n(x, t) \\ &\quad + \theta \int_0^1 r(y)M(y, x)n(y, t) dy. \end{aligned} \tag{27}$$

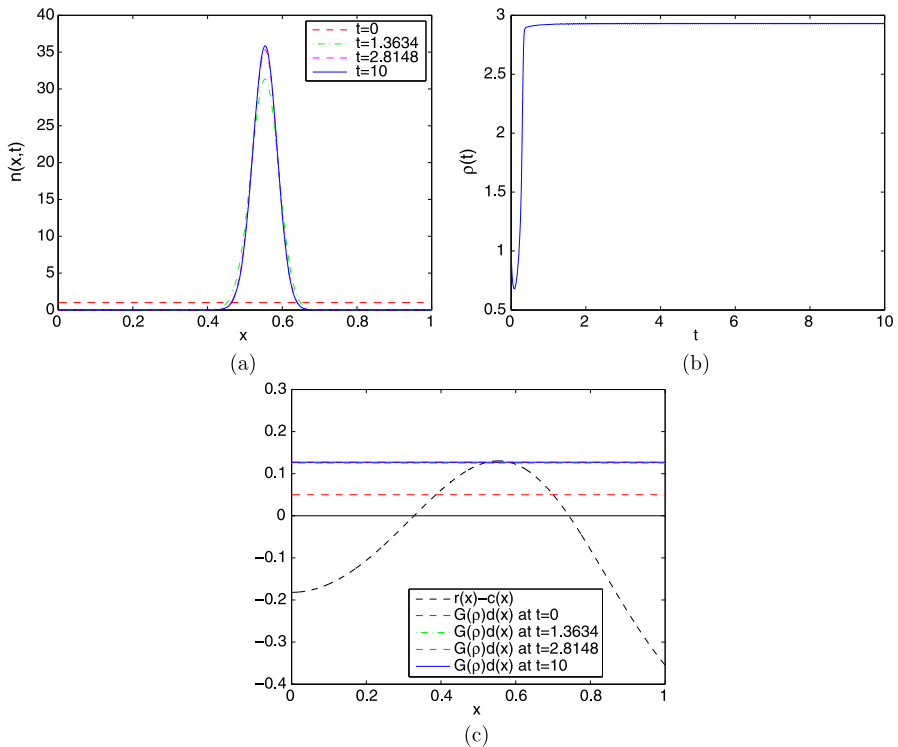


Fig. 12 Simulations of (31), using the rate parameters shown in Fig. 1(a). G is given by (19). $\epsilon = 0.01$, and $\theta = 0.1$. (a) The profiles of $n(x, t)$ at four representative times; (b) the evolution of the density; (c) the variation of the net-growth rates as the density changes in time, at the same four times used in (a) (Color figure online)

We recall that (27) is obtained from Eq. (16), by allowing for unfaithful divisions. Hence, a fraction θ of the daughter cells mutate from trait y , to a new trait x . The rate of transfer is captured in the probability density $M(y, x)$.

It turns out that if condition (17) is satisfied by $G(\rho)$, then Theorem 2 holds, namely, $\rho(t)$ remains bounded for all time t . See the Appendix for a proof.

Typically, when a model includes mutations, a natural assumption would be to allow only small mutations to occur during one division. Thus, in this case, the evolution to resistance can be interpreted as the result of a series of many small mutations over a long period of time, which changes the trait space profile of a population of cells. The term small here assesses a close distance in trait space between the original trait x and the new trait y , at least with very high probability. The degree of closeness will be specified by a small parameter ϵ . Accordingly, the mutation kernel can be written in the following form:

$$M(y, x) = \frac{1}{\epsilon} \tilde{M}(y, |y - x|/\epsilon), \quad 0 < \epsilon \ll 1. \tag{28}$$

The notation in (28) evokes the following: if x and y are within ϵ , then $M(y, x)$ is large, with $M(y, y)$ being the maximum value. Otherwise, $M(y, x) \approx 0$. Hence,

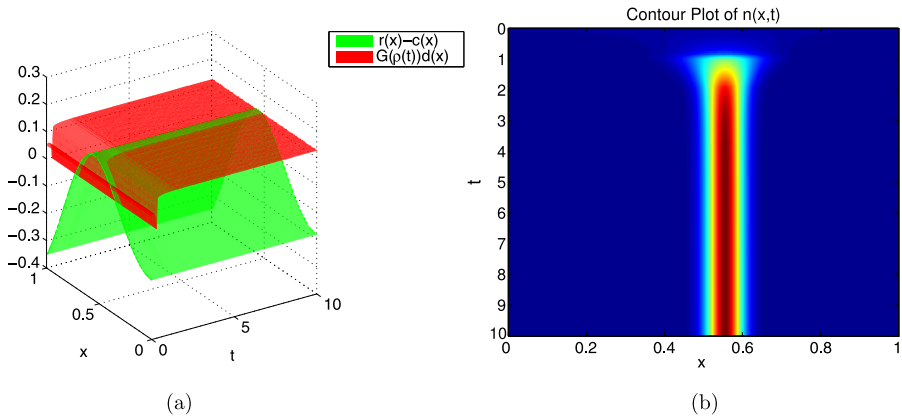


Fig. 13 Simulations of (31), with rate parameters shown in Fig. 1(a). G is given by (19). $\epsilon = 0.01$, and $\theta = 0.1$. **(a)** A surface plot of the net-growth rates; **(b)** a contour plot of $n(x, t)$ (Color figure online)

mutations are essentially limited to the interval $[y - \epsilon, y + \epsilon]$. In fact, depending on the dependence of \tilde{M} on $|y - x|/\epsilon$, this interval may even be smaller (for example, if the dependence were quadratic).

Note that there is still a y dependence outside of the distance term $|y - x|/\epsilon$ in (28), due to the fact that (4) holds for all $y \in [0, 1]$. In terms of \tilde{M} , this yields the rather technical condition that must hold for all y :

$$\int_0^{\frac{1-y}{\epsilon}} \tilde{M}(y, z) dz + \int_0^{\frac{y}{\epsilon}} \tilde{M}(y, z) dz = 1. \tag{29}$$

In writing (29) we are allowing both forward and backward mutations to occur, as we are considering this model as a basic framework. The above can be easily adapted to consider only forward mutations: simply require $\tilde{M}(y, |y - x|/\epsilon) = 0$ for $y > x$ and ignore the second term on the left-hand side in (29).

In our numerical simulations we use a Gaussian mutation kernel of the form

$$\tilde{M}(y, |y - x|/\epsilon) = K(y) \exp(-(|y - x|/\epsilon)^2). \tag{30}$$

As always, $K(y)$ is a nonnegative function chosen to ensure that (4) holds for all $y \in [0, 1]$.

Since we are interested in studying the asymptotic behavior of (27), we can rescale time t by the small parameter ϵ that appears in the mutation kernel. That is, we define the transformation $t \rightarrow t\epsilon^{-1}$ and rewrite Eq. (27) in the new time scale along with the form of the mutation kernel given by (28) as

$$\begin{aligned} \epsilon \frac{\partial n(x, t)}{\partial t} &= (r(x)(1 - \theta) - c(x) - G(\rho(t))d(x))n(x, t) \\ &\quad + \frac{\theta}{\epsilon} \int_0^1 r(y) \tilde{M}(y, |y - x|/\epsilon) n(y, t) dy. \end{aligned} \tag{31}$$

From this point on, by time we will refer to the time that is rescaled by ϵ .

Results of numerical simulations of (31) together with (30) are shown in Figs. 12 and 13. In these simulations we use the same rate and density parameters as those that were used in Figs. 3 and 4. We begin by setting the mutation length (the time-scale parameter) as $\epsilon = 0.01$, and setting the fraction of cells that undergo mutations as $\theta = 0.1$.

The dynamics that we observe from these simulations at first appear similar to what was obtained from Eq. (16). From Figs. 12(a) and 12(b) we see that the greatest density of cells lie with trait $x_* \approx 0.55425$, and the total population density converges to $\rho_* = 2.929$. However, we see that the cell population densities $n(x, t)$ no longer evolve to a point mass. Instead, they evolve into a stable distribution with a finite, nonzero variance, whose mean value will be the same value as given by the locations of the Dirac in the corresponding equation (16). One can see this either in Fig. 12(a), as the curves here corresponding to $t = 4.8727$ and $t = 10$ are vertically identical, or in Fig. 13(b), where the population values appear to be stable after $t \approx 2$. Furthermore, the line $G(\rho)d(x)$ does not become tangent to $r(x) - c(x)$ at x_* , so as not to satisfy (22) and (23). In fact, as seen most readily in Fig. 13(a), $G(\rho(t))d(x)$ stays below $r(x) - c(x)$, leaving an x interval such that $r(x) - c(x) > G(\rho(t))d(x)$. We also note that this behavior holds for all future time.

Intuitively, it is clear why $n(x, t)$ no longer approaches asymptotically a linear combination of a finite number of Dirac masses, but instead it approaches a distribution with nonzero variance. The integral term in (31) acts as a sort of diffusion operator that balances the growth of the maximal trait with the added death of mutated daughter cells in regions where $r(x) - c(x) < G(\rho)d(x)$. Even though cells are growing in the regions where $r(x) - c(x) > G(\rho)d(x)$, a fraction θ of the daughter cells are dividing unfaithfully into traits x that satisfy $r(x) - c(x) < G(\rho)d(x)$ and hence are dying. As ρ increases and the region where $r(x) - c(x) > G(\rho)d(x)$ becomes smaller, the gain in faithful divisions is countered by the loss of mutations to regions where cell populations are dying. Our limiting profile in Fig. 12(a) is the result of the balance of these two opposed forces. Note that this balance is affected both by the fraction θ of mutating cells and by the mutational distance ϵ .

We would now like to investigate the dependence of the long-time behavior of (31) on the parameters θ and ϵ . We perform numerical simulations using the trait parameters as in Fig. 1(a) and the density from Eq. (19). First, we fix $\epsilon = 0.01$ and vary θ . The results are shown in Fig. 14. Note that we only plot n at time $t = 10$, since we have checked that $n(x, t)$ is no longer significantly changing for $t > 10$. We observe two basic phenomena in Fig. 14. First, as we allow a higher average fraction of cells to undergo unfaithful division, the distribution of cells about the maximum trait x_* widens. This is an intuitive result, since increasing the fraction of cells mutating away allows for a greater variability of traits. Secondly, the total mass is nearly constant at $\rho_f := \rho(t = 10) \approx 2.9$, but does slightly decrease monotonically as θ increases. Hence, the main effect in this case seems to be increasing the variance in the trait x of the cell population with mean value x_* . In other words, as θ increases, the heterogeneity in the tumor also increases, with a very slight effect on the overall mass of cells. To understand this, note that ϵ is small in the simulation, so that mutations, when they occur, are localized. Hence, even when a large fraction of cells is mutating

Fig. 14 Simulations of (31), at time $t = 10$. Plotted are $n(x, 10)$ obtained using rate parameters shown in Fig. 1(a). G is given by (19). $\theta = 0.1, 0.4, 0.7, 1$. For all plots, $\epsilon = 0.01$ is fixed (Color figure online)

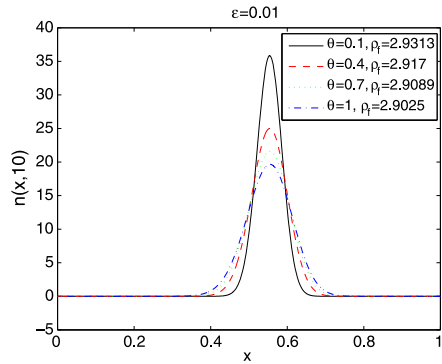
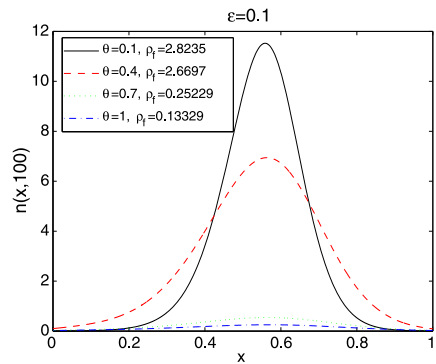


Fig. 15 Simulations of (31) at time $t = 100$. All other parameters are identical to those used in Fig. 14 (Color figure online)



(θ larger), they cannot mutate to a point that is too far away. By the continuity of all the growth/death parameters, the increase in apoptosis to those cells who mutate away from the maximum is small, hence yielding only a small decrease in ρ_f .

We repeat our simulations with a larger value of $\epsilon = 0.1$. We note that in this case, it seemed to take a longer amount of time for the simulations to reach the steady state. After $t = 100$, the simulations no longer observably varied, and hence we define $\rho_f := \rho(t = 100)$. The results of these simulations are shown in Fig. 15. Once again, the variance of cells about the maximum trait x_* increases as θ increases. However, in this case, the final densities ρ_f decrease much more as θ increases. Since ϵ is larger, daughter cells are allowed to mutate much farther away in an unfaithful division when compared with the smaller ϵ simulations. Hence, these cells jump to regions in trait space x that are much farther away from the maximum x_* . Here, the net growth rate is very negative, causing these cells to die quickly and hence have a lower ρ_f when compared to the previous case of $\epsilon = 0.01$. The overall effect leads to a decrease in the overall steady-state populations.

From Figs. 14 and 15 we conclude that both parameters ϵ and θ affect the amount of heterogeneity seen in the cell population. For a fixed ϵ , we see that as θ increases, the overall population will increase in variance and decrease in steady-state density. The rate of decrease of this density, ρ_f , is strongly affected by the ϵ parameter. Smaller values of ϵ will cause small variation in ρ_f as θ varies, but as ϵ increases, so does the volatility of ρ_f with respect to θ . We note that increasing the fraction

of mutating cells can act to decrease the total mass of the tumor. This effect is more pronounced for more widely varying mutations, that is, in models with larger values of ϵ . We finally note that as $\epsilon \rightarrow 0^+$, the dynamics of (31) approaches the dynamics of (16). We refer interested readers to Lorz et al. (2013), where a rigorous analysis of such a limit is undertaken. However, here we do not consider such a limit to be appropriate from a modeling point of view, as our goal was to achieve local heterogeneity, which cannot be achieved with Eq. (16). Accordingly, our study only considers the case of a finite, nonzero ϵ .

4 Discussion

The goal of this paper was to develop a modeling framework for MDR that can qualitatively capture the complexity of the underlying dynamics. To achieve this goal, we introduce a hierarchy of models, which we have studied analytically and numerically.

Our study starts with a simple uncoupled system of ODEs parameterized by the resistance level x , and given by Eq. (8). We demonstrate that this model can capture the selection of a finite number of traits. On the down side, in such models, the total cell density always either diverges or dies off, an outcome that contradicts the biology.

This motivated the introduction of a cooperative/competitive density dependence into the model, which led to Eq. (16). In this case, the emerging dynamics was similar to (8), in that the limiting distribution is a finite collection of Dirac masses. Now though, under mild conditions on the density dependence (see (17)), the total density remains bounded. Furthermore, we demonstrated that the final selected trait (or traits) can be different between (8) and (16). While the model (16) has clear benefits in comparison with (8), the homogeneity of the cell populations is in contrast to the biological literature, as discussed in Sect. 1.

Finally, we introduced a mutation mechanism into the model via an integral term, given by (31). The dynamics of this model were then demonstrated to be similar to those in (16), in that the population densities were maximal at the same trait values x , and the population density remains bounded. However, in this mutation/selection model, the Dirac masses are replaced in the limit by distributions with nonzero variance. That is, there exists a continuum of traits that are stable for all time. This is interpreted as tumor heterogeneity, which was the desired outcome.

Mathematical models offer ways to predict the net-growth rate during and after the administration of a treatment. These mathematical models and their outcomes each have their own definitions and assumptions of growth. What function best describes the growth dynamics of cancer, and what are the consequences of using different growth descriptions in MDR? In this work, we have developed an alternative cancer growth model to the exponential, logistic, or Gompertzian growth, which also integrates resistance level. This work has implications in the clinical setting for solid tumor and metastasis studies, and for more details, one should see our recent published works (Lavi et al. 2013, 2014). This issue is a critical step toward the ability to predict the dynamics of drug resistance and intratumoral heterogeneity in cancer during and after therapy. Accordingly, we view the model (31) as a basic framework that can be extended to model more realistic MDR mechanisms. In particular, providing experimentally solid estimates for the birth and death rates ($r(x)$, $d(x)$), and

$c(x)$) along with the density dependencies ($f(\rho)$ and $g(\rho)$) will be the focus of future work.

Acknowledgements We would like to thank George Leiman for editorial assistance. The work was supported by the Intramural Research Program of the National Institutes of Health, Center for Cancer Research, National Cancer Institute and was supported in part by a seed grant from the UMD-NCI Partnership for Cancer Technology. The work of D.L. was supported in part by the joint NSF/NIGMS program under Grant Number DMS-0758374 and by Grant Number R01CA130817 from the National Cancer Institute.

Appendix A

Proposition 1 Consider the integro-differential equation (6). If $n(x, 0) \geq 0$ for all $x \in [0, 1]$, then

$$n(x, t) \geq 0 \quad \forall t \in \mathbb{R}_+.$$

Proof The global existence of continuously differentiable solutions of (1) can be obtained following standard arguments (see Perthame 2007). For the positivity of n , since $n \geq 0$ at $t = 0$, due to its continuity, if there exists a t_* for which $n(x, t_*) = 0$ for some $x \in [0, 1]$ (and $n(x, t) > 0$ for $t < t_*$), then $n(y, t_*) \geq 0$ for all y . Hence, by (6),

$$\frac{\partial n(x, t_*)}{\partial t} = \theta \int_0^1 r(y)M(y, x)n(y, t_*) \, dy \geq 0, \tag{32}$$

which implies that $n(x, t_*)$ is nondecreasing at t_* . Consequently, $n(x, t)$ cannot pass through 0, as stated. □

Proof of Theorem 1 We follow the proof of Lorz et al. (2013), Lemma 2.2. Consider system (8). If $r(x) - c(x) - d(x) < 0$ for all $x \in [0, 1]$, then due to the positivity of $n(x, t)$, $\frac{\partial n(x,t)}{\partial t} < 0$ for all $x \in [0, 1]$. Hence, $n(x, t) \xrightarrow[t \rightarrow \infty]{} 0$ in $[0, 1]$. By Lebesgue’s Dominated Convergence Theorem, this implies that $\rho(t) \rightarrow 0$ as $t \rightarrow \infty$.

If, on the other hand, there exists x_* such that $r(x_*) - c(x_*) - d(x_*) = 0$, then these are fixed points of (8), and hence,

$$n(x_*, t) = n(x_*, 0) \quad \forall t \in \mathbb{R}_+.$$

Now suppose that there exists $x \in [0, 1]$ such that $r(x) - c(x) - d(x) > 0$. By the continuity of the growth parameters and the compactness of $[0, 1]$, $r(x) - c(x) - d(x)$ achieves its maximum, say at $\{x_i\}_{i=1}^m$. We note that it is possible that $m = \infty$, or even that the set $\{x_i\}_{i=1}^m$ is uncountable (in which case our notation should be altered).

To see that $\rho(t) \xrightarrow[t \rightarrow \infty]{} \infty$, fix $x_j \in \{x_i\}_{i=1}^m$ such that $n(x_j, 0) > 0$ (as the points where $n = 0$ do not contribute to the growth). Then for all $0 < \lambda < r(x_j) - c(x_j) - d(x_j)$, there exists γ_λ such that

$$r(x) - c(x) - d(x) \geq \lambda > 0 \quad \forall x \in [x_j - \gamma_\lambda, x_j + \gamma_\lambda].$$

Let $h_\lambda(t) := \int_{x_j-\gamma_\lambda}^{x_j+\gamma_\lambda} n(x, t) \, dx$. Then

$$\frac{d}{dt} h_\lambda(t) = \int_{x_j-\gamma_\lambda}^{x_j+\gamma_\lambda} [r(x) - c(x) - d(x)] n(x, t) \, dx \geq \lambda \int_{x_j-\gamma_\lambda}^{x_j+\gamma_\lambda} n(x, t) \, dx = \lambda h_\lambda(t),$$

so that, for a positive constant $h(0)$,

$$h_\lambda(t) \geq h(0)e^{\lambda t}. \tag{33}$$

As $\rho(t) = \int_0^1 n(x, t) \, dx \geq h_\lambda(t)$, (33) implies that $\rho(t) \xrightarrow{t \rightarrow \infty} \infty$, as desired. To find the limiting distribution, note that for $x \notin \{x_i\}_{i=1}^m$, choose λ such that

$$r(x) - c(x) - d(x) < \lambda < r(x_j) - c(x_j) - d(x_j).$$

Then,

$$\frac{n(x, t)}{\rho(t)} = \frac{n(x, 0)e^{[r(x)-c(x)-d(x)]t}}{\rho(t)} \leq \frac{n(x, 0)}{h(0)} e^{[r(x)-c(x)-d(x)-\lambda]t} \xrightarrow{t \rightarrow \infty} 0. \tag{34}$$

As $\int_0^1 \frac{n(x,t)}{\rho(t)} \, dx = 1$, for all time t , we have the desired result, namely

$$\lim_{t \rightarrow \infty} \frac{n(x, t)}{\rho(t)} = \sum_{i=1}^m a_i \delta(x - x_i),$$

with $\sum_{i=1}^m a_i = 1$. If the number of maximizers is uncountable, a similar result will hold for a continuous measure. □

Proof of Theorem 2 Let $n(x, t)$ satisfy (16). By Proposition 1, since $n(x, t) \geq 0$, $\rho(t) \geq 0$ as well. Let r_M, c_m , and d_m be constants such that $r(x) \leq r_M, c(x) \geq c_m > 0$, and $d(x) \geq d_m > 0$, and recall that $G \geq 0$. Hence, $\rho'(t)$ can be bounded above by

$$\frac{d\rho(t)}{dt} = \int_0^1 [r(x) - c(x) - G(\rho(t))d(x)] n(x, t) \, dx \leq [r_M - c_m - G(\rho(t))d_m] \rho(t).$$

Since $G(\rho) \xrightarrow{\rho \rightarrow \infty} \infty$, there exists ρ_M such that $\rho(0) \leq \rho_M$ and $r_M - c_m - G(\rho_M)d_m < 0$. This implies that at $\rho = \rho_M, \rho'(t) < 0$, and hence $\rho(t) \leq \rho_M$. □

References

Bellomo, N. (1997). Nonlinear models and problems in applied sciences from differential quadrature to generalized collocation methods. *Math. Comput. Model.*, 26(4), 13–34.

Birkhead, B. G., Rakin, E. M., Gallivan, S., Dones, L., & Rubens, R. D. (1987). A mathematical model of the development of drug resistance to cancer chemotherapy. *Eur. J. Cancer Clin. Oncol.*, 23(9), 1421–1427.

Bozic, I., Allen, B., & Nowak, M. A. (2012). Dynamics of targeted cancer therapy. *Trends Mol. Med.*, 18(6), 311–316.

- Brimacombe, K. R., Hall, M. D., Auld, D. S., Inglese, J., Austin, C. P., Gottesman, M. M., & Fung, K. L. (2009). A dual-fluorescence high-throughput cell line system for probing multidrug resistance. *Assay Drug Dev. Technol.*, 7(3), 233–249.
- Calsina, À., & Cuadrado, S. (2000). A model for the adaptive dynamics of the maturation age. *Ecol. Model.*, 133, 33–43.
- Calsina, À., & Cuadrado, S. (2004). Small mutation rate and evolutionary stable strategies in infinite dimensional adaptive dynamics. *J. Math. Biol.*, 48, 135–159.
- Champagnat, N., Ferrière, R., & Méléard, S. (2006). Unifying evolutionary dynamics: from individual stochastic processes to macroscopic models. *Theor. Popul. Biol.*, 69(3), 297–321.
- Coldman, A. J., & Goldie, J. H. (1985). Role of mathematical modeling in protocol formulation in cancer chemotherapy. *Cancer Treat. Rep.*, 69(10), 1041–1048.
- Coldman, A. J., & Goldie, J. H. (1986). A stochastic model for the origin and treatment of tumors containing drug-resistant cells. *Bull. Math. Biol.*, 48(3–4), 279–292.
- Desvillettes, L., Jabin, P. E., Mischler, S., & Raoul, G. (2008). On selection dynamics for continuous structured populations. *Commun. Math. Sci.*, 6(3), 729–747.
- Diekmann, O., Jabin, P. E., Mischler, S., & Perthame, B. (2005). The dynamics of adaptation: an illuminating example and a Hamilton–Jacobi approach. *Theor. Popul. Biol.*, 67(4), 257–271.
- Fister, K. R., & Panetta, J. C. (2003). Optimal control applied to competing chemotherapeutic cell-kill strategies. *SIAM J. Appl. Math.*, 63(6), 1954–1971.
- Fodal, V., Pierobon, M., Liotta, L., & Petricoin, E. (2011). Mechanisms of cell adaptation: when and how do cancer cells develop chemoresistance? *Cancer J.*, 17(2), 89–95.
- Forys, U., & Marciniak-Czochra, A. (2003). Logistic equations in tumor growth modeling. *Int. J. Appl. Math. Comput. Sci.*, 13(3), 317–325.
- Gillet, J. P., & Gottesman, M. M. (2010). Mechanisms of multidrug resistance in cancer. *Methods Mol. Biol.*, 596, 47–76.
- Goldie, J. H., & Coldman, A. J. (1979). A mathematical model for relating the drug sensitivity of tumors to their spontaneous mutation rate. *Cancer Treat. Rep.*, 63(11–12), 1727–1733.
- Goldie, J. H., & Coldman, A. J. (1983a). A model for resistance of tumor cells to cancer chemotherapeutic agents. *Math. Biosci.*, 65, 291–307.
- Goldie, J. H., & Coldman, A. J. (1983b). Quantitative model for multiple levels of drug resistance in clinical tumors. *Cancer Treat. Rep.*, 67(10), 923–931.
- Goldie, J. H., & Coldman, A. J. (1998). *Drug resistance in cancer: mechanisms and models*. Cambridge: Cambridge University Press.
- Goldie, J. H., Coldman, A. J., & Gudauskas, G. A. (1982). Rationale for the use of alternating non-cross resistant chemotherapy. *Cancer Treat. Rep.*, 66(3), 439–449.
- Grantab, R., Sivananthan, S., & Tannock, I. F. (2006). The penetration of anticancer drugs through tumor tissue as a function of cellular adhesion and packing density of tumor cells. *Cancer Res.*, 66(2), 1033–1039.
- Hakanson, M., Kobel, S., Lutolf, M. P., Textor, M., Cukierman, E., & Charnley, M. (2012). Controlled breast cancer microarrays for the deconvolution of cellular multilayering and density effects upon drug responses. *PLoS ONE*, 7(6), e40141.
- Harnevo, L. E., & Agur, Z. (1991). The dynamics of gene amplification described as a multitype compartmental model and as a branching process. *Math. Biosci.*, 103(1), 115–138.
- Jackson, T. L., & Byrne, H. (2000). A mathematical model to study the effects of drug resistance and vasculature on the response of solid tumors to chemotherapy. *Math. Biosci.*, 164(1), 17–38.
- Khain, E., & Sander, L. M. (2006). Dynamics and pattern formation in invasive tumor growth. *Phys. Rev. Lett.*, 96(18), 188103.
- Kimmel, M., & Axelrod, D. E. (1990). Mathematical models of gene amplification with applications to cellular drug resistance tumorigenicity. *Genetics*, 125(3), 633–644.
- Komarova, N. (2006). Stochastic modeling of drug resistance in cancer. *J. Theor. Biol.*, 239(3), 351–366.
- Komarova, N., & Wodarz, D. (2005). Drug resistance in cancer: principles of emergence and prevention. *Proc. Natl. Acad. Sci. USA*, 102(27), 9714–9719.
- Kreso, A., O’Brien, C. A., van Galen, P., Gal, O. I., Notta, F., et al. (2013). Variable clonal repopulation dynamics influence chemotherapy response in colorectal cancer. *Science*, 339(6119), 543–548.
- Laird, A. K. (1964). Dynamics of tumor growth. *Br. J. Cancer*, 18(3), 490–502.
- Lavi, O., Gottesman, M. M., & Levy, D. (2012). The dynamics of drug resistance: a mathematical perspective. *Drug Resist. Updat.*, 15(1–2), 90–97.
- Lavi, O., Greene, J. M., Levy, D., & Gottesman, M. M. (2013). The role of cell density and intratumoral heterogeneity in multidrug resistance. *Cancer Res.*, 73(24), 7168–7175.

- Lavi, O., Greene, J. M., Levy, D., & Gottesman, M. M. Simplifying the complexity of resistance heterogeneity in metastasis, Trends in Molecular Medicine (2014, accepted).
- Ledzewicz, U., & Schattler, H. (2006). Drug resistance in cancer chemotherapy as an optimal control problem. *Discrete Contin. Dyn. Syst.*, 6(1), 129–150.
- Long, H., Han, H., Yang, B., & Wang, Z. (2003). Opposite cell density-dependence between spontaneous and oxidative stress-induced apoptosis in mouse fibroblast L-cells. *Cell. Physiol. Biochem.*, 13(6), 401–414.
- Lorz, A., Mirrahimi, S., & Perthame, B. (2011). Dirac mass dynamics in multidimensional nonlocal parabolic equations. *Commun. Partial. Differ. Equ.*, 36(6), 1071–1098.
- Lorz, A., Lorenzi, T., Hochberg, M., Clairambault, J., & Perthame, B. (2013). Populational adaptive evolution, chemotherapeutic resistance and multiple anti-cancer therapies. *Math. Model. Num. Anal.*, 47(2), 377–399.
- Magal, P., & Webb, G. F. (2000). Mutation, selection and recombination in a model of phenotype evolution. *Discrete Contin. Dyn. Syst.*, 6(1), 221–236.
- Marusyk, A., & Cancer, K. P. (2013). Cancer cell phenotypes, in fifty shades of grey. *Science*, 339(6119), 528–529.
- Michelson, S., & Slate, D. (1992). A mathematical model of the P-glycoprotein pump as a mediator of multidrug resistance. *Bull. Math. Biol.*, 54(6), 1023–1038.
- Nagane, M., Coufal, F., Lin, H., Bögl, O., Cavenee, W. K., & Huang, H. J. (1996). A common mutant epidermal growth factor receptor confers enhanced tumorigenicity on human glioblastoma cells by increasing proliferation and reducing apoptosis. *Cancer Res.*, 56(21), 5079–5086.
- Norton, L., & Simon, R. (1977a). Tumor size, sensitivity to therapy, and design of treatment schedules. *Cancer Treat. Rep.*, 61(7), 1307–1317.
- Norton, L., & Simon, R. (1977b). The growth curve of an experimental tumor following radiotherapy. *J. Natl. Cancer Inst.*, 58(6), 1735–1741.
- Norton, L., & Simon, R. (1986). The Norton–Simon hypothesis revisited. *Cancer Treat. Rep.*, 70(1), 163–169.
- Panetta, J. C. (1998). A mathematical model of drug resistance: heterogeneous tumors. *Math. Biosci.*, 147(1), 41–61.
- Perthame, B. (2007). *Transport equations in biology, frontiers in mathematics*. Basel: Birkhäuser.
- Perthame, B., & Barles, G. (2008). Dirac concentrations in Lotka–Volterra parabolic PDEs. *Indiana Univ. Math. J.*, 57(7), 3275–3301.
- Qiao, L., & Farrell, G. C. (1999). The effects of cell density, attachment substratum and dexamethasone on spontaneous apoptosis of rat hepatocytes in primary culture. *In Vitro Cell. Dev. Biol., Anim.*, 35(7), 417–424.
- Saeki, K., Yuo, A., Kato, M., Miyazono, K., Yazaki, Y., & Takaku, F. (1997). Cell density-dependent apoptosis in HL-60 cells, which is mediated by an unknown soluble factor, is inhibited by transforming growth factor beta1 and overexpression of Bcl-2. *J. Biol. Chem.*, 272(32), 20003–20010.
- Saunders, N. A., Simpson, F., Thompson, E. W., Hill, M. M., Endo-Munoz, L., et al. (2012). Role of intratumoral heterogeneity in cancer drug resistance: molecular and clinical perspectives. *EMBO J.*, 4(8), 675–684.
- Schuster, R., & Schuster, H. (1995). Reconstruction models for the Ehrlich ascites tumor of the mouse. *Math. Pop. Dyn.*, 2, 335–348.
- Stein, A. M., Demuth, T., Mobley, D., Berens, M., & Sander, L. M. (2007). A mathematical model of glioblastoma tumor spheroid invasion in a three-dimensional in vitro experiment. *Biophys. J.*, 921, 356–365.
- Tomasetti, C., & Levy, D. (2010). An elementary approach to modeling drug resistance in cancer. *Math. Biosci. Eng.*, 7(4), 905–918.
- Weaver, V. M., Lelièvre, S., Lakins, J. N., Chrenek, M. A., Jones, J. C., Giancotti, F., Werb, Z., & Bissell, M. J. (2002). Beta4 integrin-dependent formation of polarized three-dimensional architecture confers resistance to apoptosis in normal and malignant mammary epithelium. *Cancer Cell*, 2(3), 205–216.
- Zahir, N., & Weaver, V. M. (2004). Death in the third dimension: apoptosis regulation and tissue architecture. *Curr. Opin. Genet. Dev.*, 14(1), 71–80.